Electric field and temperature dependence of the local structural disorder in the lead-free ferroelectric $Na_{0.5}Bi_{0.5}TiO_3$: An EXAFS study

Badari Narayana Rao,[1] Luca Olivi,[2] Vasant Sathe,[3] and Rajeev Ranjan[1,*]

[1]*Department of Materials Engineering, Indian Institute of Science, Bangalore 560012, India*

[2]*Elettra-Sincrotrone Trieste S.C.p.A., Strada Statale 14 km 163.5, 34194 Basovizza, Trieste, Italy*

[3]*UGC-DAE Consortium for Scientific Research, University Campus, Khandwa Rd., Indore 452017, India*

(Received 6 November 2015; published 11 January 2016)

The complex nature of the structural disorder in the lead-free ferroelectric $Na_{1/2}Bi_{1/2}TiO_3$ has a profound impact on the perceived global structure and polar properties. In this paper, we have investigated the effect of electric field and temperature on the local structure around the Bi and Ti atoms using extended x-ray absorption fine structure. Detailed analysis revealed that poling brings about a noticeable change in the bond distances associated with the Bi-coordination sphere, whereas the Ti coordination remains unaffected. We also observed discontinuity in the Bi-O bond lengths across the depolarization temperature of the poled specimen. These results establish that the disappearance of the monoclinic-like (Cc) global distortion, along with the drastic suppression of the short-ranged in-phase octahedral tilt after poling [B. N. Rao *et al.*, Phys. Rev. B **88**, 224103 (2013)] is a result of the readjustment of the A-O bonds by the electric field, so as to be in conformity with the rhombohedral $R3c$ structure.

DOI: 10.1103/PhysRevB.93.024106

I. INTRODUCTION

$Na_{0.5}Bi_{0.5}TiO_3$ (NBT) and its derivatives are among the most extensively investigated lead-free piezoelectrics. Though discovered more than six decades ago, research in the past 15 years has revealed great complexity in the structure and phase transition behavior of NBT. While the earlier bulk-diffraction-technique-based studies reported a rhombohedral ($R3c$) structure [1,2], a considerable departure from the $R3c$ structure was observed in studies investigating the local structure [3–7]. A modulated domain structure of the real space period of ~ 4 nm was suggested by Thomas *et al.* [8]. Balagurov *et al.*, on the other hand, argued about the incommensurate modulation of the $R3c$ phase along the four-fold axis of the precursor tetragonal phase [5]. X-ray and neutron diffuse scattering experiments show a remarkable asymmetry in the diffuse scattering, which is not expected if the system is truly rhombohedral [3,5,8]. These disorders have been attributed to small perpendicular displacements of Bi^{+3} cations away from the polar $\langle 111\rangle_{pc}$ direction to improve its coordination environment [3,9]. Local structure analysis using x-ray absorption fine structure (XAFS) and neutron total scattering have revealed that, although both Na and Bi occupy the same Wyckoff site, the bonding characteristics of Na and Bi atoms induce very different local Bi-O and Na-O bond lengths [4,6]. One of the highlights of such studies is the demonstration that the shortest Bi-O bond is about 0.3 Å shorter than what has been calculated based on the average crystal structure analysis [4]. Neutron pair distribution analysis has also revealed the presence of an anomalous Bi-O distance of 3.2 Å in NBT which cannot be accounted for by the $R3c$ structure [6]. These results support the bond-valence calculations performed by Jones and Thomas who showed that the Bi^{+3} is heavily under-bonded in the average rhombohedral structure, as revealed by bulk diffraction techniques [2]. Recent high-resolution x-ray diffraction studies on single crystals and the powder of NBT have shown that its symmetry must be lower than $R3c$, and proposed a monoclinic Cc structure [10,11]. Gorfman *et al.* have also cited the absence of well-defined domain walls in optical birefringence study, expected for a rhombohedral structure, as a basis for the presence of a lower symmetry of NBT [12]. Ge *et al.* suggested the Cc phase to be an extrinsic (skin) effect, which was caused by the presence of strong random electric fields [13]. Electron diffraction studies, have revealed additional weak superlattice reflections of the odd-odd-even type $(1/2\{ooe\}_{pc}$, notation in accordance with Glazer's scheme [14,15]), along with diffuse rodlike scattering, indicating a presence of thin sheets of $a^0a^0c^+$ octahedral tilt embedded in the rhombohedral matrix [16–18]. Levin and Reaney have suggested an average tilt configuration of $a^-a^-c^+/\,a^-a^-c^-$, which is consistent with a monoclinic Cc distortion [19]. In a bid to correlate the bulk diffraction results and the electron diffraction results, Rao *et al.* have shown a one-to-one correspondence between the perceived monoclinic distortion on the global scale and the presence of short-range order in-phase tilted octahedra [20]. On the application of strong electric field (poling), the spatial correlation of the short-ranged in-phase tilted octahedra decreases dramatically and the global structure appears as pure rhombohedral in x-ray diffraction (XRD). Recently, Usher *et al.* carried out *in situ* electric-field-dependent x-ray total scattering studies on NBT and showed that electric field causes an ordering of the local Bi displacements and the deviations of the A cation from the average rhombohedral axis were suppressed [21]. These studies clearly prove that a strong correlation exists between the presence of short-range structural disorder and its implication on the dielectric, ferroelectric, and the global structure of NBT. So far, such a correlation has not been established on the local (atomic) scale using EXAFS. It is unclear if the occurrence of the in-phase octahedral tilt is self-driven or if it is a result of localized displacement of the A-site cations away from the polar direction, as suggested by Kreisel *et al.* [3].

In this paper, we settle this issue by carrying out a comparative study of the local structure of the unpoled and poled NBT

*rajeev@materials.iisc.ernet.in

using extended x-ray absorption spectroscopy (EXAFS). This technique has the advantage of selectively offering information on the coordination environment of any specific element in the specimen such as the bond length, coordination number, and so on. In addition, it is sensitive to an order below Ångstrom scale and measures local effects that are inaccessible to many other experimental techniques. Earlier, Shuvaeva *et al.* reported on the EXAFS study on the Bi L_{III}-edge and Ti K-edge spectra of unpoled NBT [4]. While their study revealed quantitative information about the Bi-O distances, the Ti-O coordination was analyzed only in a qualitative manner, using Ti-K-edge x-ray absorption near edge spectrum (XANES) data. Our results reveal that the electric field has a significant influence on the atomic distances associated with the Bi coordination, but not on the Ti coordination. The slight readjustment of the Bi-O bonds on poling is associated with the tendency of the electric field to align the atomic displacements in conformity with the *R*3*c* structure. These results also suggest that the occurrence of short-range in-phase octahedral tilt is related to the nonrhombohedral displacements of the *A*-site cations. A small anomaly in the bond lengths associated with the Bi coordination was found when the poled specimen was heated through the depolarization temperature ($T_d \sim 200\,^{\circ}$C), confirming the positional disorder on the *A* site to be the primary factor leading to the complex structure-property relationship in NBT.

II. EXPERIMENTAL PROCEDURE

NBT was prepared by the conventional solid-state route. Dried powders of high purity Bi_2O_3, Na_2CO_3, and TiO_2 were taken in stoichiometric ratios and mixed in a planetary ball mill for 10 hours in acetone medium, using zirconia vials and balls. The mixture was then dried and calcined at 900° C for 2 hours in air. The calcined powder was mixed with 2% PVA solution and then pressed into pellets under a uniaxial pressure of 100 MPa. These pellets were then cold isostatically pressed at 300 MPa to obtain high density. Sintering was carried out at 1200° C for 2 hours in air. The densities of the pellets were measured using the Archimedes principle, and the average density after sintering was found to be around 96–97% of the theoretical density. The sintered pellets were painted with Ag paste for electrical contact. Electric poling was carried out at room temperature by applying a dc field of 60 kV/cm for 10 minutes on the sample which was dipped in silicone oil. The Bi L_{III}-edge and Ti K-edge XAFS spectra of the NBT specimen were collected at the EXAFS beamline 11.1 at the ELETTRA Synchrotron Light Laboratory, Basovizza, Italy. The spectra was collected over an energy range of 13 118–14 300 eV for Bi L_{III}-edge, and 4666 eV–5500 eV for Ti K-edge. The data were collected three times and then averaged to reduce the noise and improve the statistics. To obtain EXAFS spectra from the poled specimen, the poled pellet was manually polished to remove the silver electrode and later crushed into a fine powder in a mortar and pestle. The raw data collected was background subtracted and normalized to extract EXAFS as a function of *k* through a series of steps using the ATHENA software [22], which implements the "AUTOBK" algorithm for the reduction [23]. Once the data reduction was carried out, the fitting of the spectrum with a specific model was carried out with the help

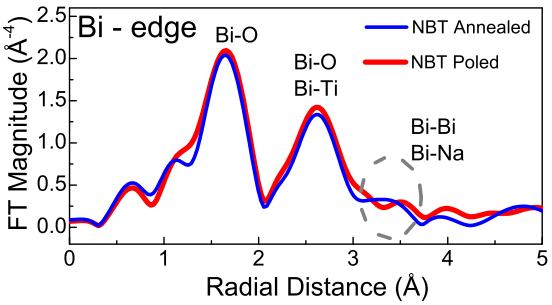

FIG. 1. Comparison of the room temperature Bi L_{III}-Edge EXAFS spectra of poled and unpoled NBT.

of the software ARTEMIS [22]. The software first computes a theoretical spectrum from a given model using the ATOMS and FEFF6 programs [24–26]. The analysis consists of modeling χ(k) in terms of the sum of the ''paths," with the XAFS contribution from each path being guided by the calculation from FEFF. In the present work, the EXAFS spectrum of Bi L_{III}-edge and Ti K-edge of NBT were simultaneously fit with different structural models to understand the effect of electric field and temperature on the local structure of NBT.

III. RESULTS

A. Poling-induced changes in the room temperature EXAFS spectra

Figure 1 shows a comparison of the Fourier transformed Bi L_{III}-edge EXAFS spectra for the poled and unpoled NBT, collected at room temperature. For the first two peaks, it can be seen that there is no noticeable difference between the two patterns. These first two peaks comprise mainly of the first and second nearest-neighbor bonds, namely, the Bi-O and Bi-Ti bonds. However, there is a noticeable change in the third peak around 3.5 Å, which comprises the Bi-Bi and Bi-Na bonds. The broad feature of this peak in the unpoled sample gets suppressed to some extent, and appears sharper in the poled sample. On the other hand, we can see from Fig. 2 that there is no observable difference between the Fourier-transformed Ti K-edge EXAFS spectra of the poled and unpoled NBT, even up to a distance of 5 Å. This implies that the Ti coordination is not affected by the application of the electric field. Comparing Figs. 1 and 2, it can be seen that the peak corresponding to the Bi-Ti bonds in Bi-edge spectra is at ∼2.6 Å, whereas it is at

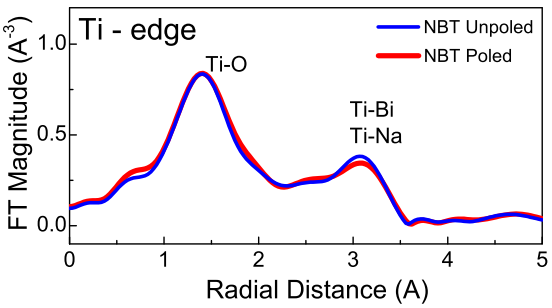

FIG. 2. Comparison of the room temperature Ti K-Edge EXAFS spectra of poled and unpoled NBT.

~3 Å in the Ti-edge spectra. This difference occurs because the peaks in the magnitude of χ(R) are not directly related to the interatomic distance. The photoelectron undergoes a phase shift when it interacts with the nuclei of the absorber atom and those of the coordinating atoms, which causes a shift in the peak position of approximately −0.5 Å. This is the reason that pictorially the Bi-Ti bond appears at a lower distance in the Bi-edge spectra than in the Ti-edge spectra.

Fitting room temperature EXAFS spectra of poled and unpoled NBT with the R3c model

Since the bulk structure of poled sample of NBT unambiguously shows *R*3*c* structure [27,28], we tried to fit the Bi L_{III}-edge and Ti K-edge spectra with the *R*3*c* model for both poled and unpoled samples. A reasonably good fit with this structural model would imply that the local structure is indeed rhombohedral in nature. The Bi L_{III}-edge and Ti K-edge spectra were fit simultaneously so that the common Bi-Ti bonds involved in both the spectra would lead to reduction in the number of variables used for the refinement. The *k*-range considered for the Bi L_{III}-edge spectra was from 3 to 11 $Å^{-1}$ whereas for the Ti K-edge spectra, it was from 3 to 11.7 $Å^{-1}$. The *R* range for both the spectra was set as 1 to 3.5 Å. There is a limitation on the number of structural parameters that are involved in the refinement, which should not exceed the number of independent points (N_I) in the spectra. N_I is proportional to the *k* range and *R* range of the EXAFS spectra considered in the refinement, and is defined by the Nyquist criterion as $= \frac{2\Delta k \Delta R}{\pi} + 1$ [29,30]. In the present case, when the combined fitting of both the Bi L_{III}-edge and Ti K-edge data is considered, N_I would be equal to 26.26. We found that to define our rhombohedral structure adequately; we needed to consider at least 17 variables, which is well below N_I. To test the *R*3*c* model with these data, we created theoretical fitting standards using the ATOMS software, loaded with an inbuilt program FEFF, version 6.0, to calculate the theoretical EXAFS pattern [31]. The starting cell parameters for the *R*3*c* model were taken from the Rietveld analysis result of the XRD pattern of poled NBT [28]. The software ARTEMIS was used to refine the variable parameters of all the paths within the constraints of the *R*3*c* space group, so that the theoretical EXAFS pattern would match with the observed data [22]. Only single scattering paths were considered for the fit, as the inclusion of multiple scattering paths did not help to improve the fit. The details of various paths used in fitting the Bi L_{III}-edge and Ti K-edge data are summarized in Table I and can be visualized from Fig. 3.

Since NBT contains *A*-site disorder (with 'Na' and 'Bi' sharing the same site), we cannot define the initial *R*3*c* cell in a straightforward manner. This is because the ATOMS software, which is used to feed the starting parameters of the *R*3*c* structure, does not allow for sharing of the atomic sites [Figs. 3(b) and 3(d)], which would then complicate the calculation of the different scattering paths. Hence, to effectively define the *A*-site disorder in our model, we follow the method described in Chapters 13 and 16 of Ref. [32]. For the Bi L_{III}-edge, two cells are considered wherein one has bismuth atoms both at the core and all the other *A* sites, whereas the other cell has a bismuth atom at the core and all the other *A* sites filled with Na alone. Then the average signal of these two cells is considered as the net theoretical EXAFS signal. Similarly, for the Ti K-edge, one cell with all the *A* sites containing only Bi, and the other cell containing only Na was considered, and then the average of both the signals was considered as the net theoretical spectra. In addition, ARTEMIS does not have the option to constrain the path lengths to adhere to a particular space group. Hence, additional constraints related to *R*3*c* symmetry were manually fed into the software. To do this, all the path lengths were described in terms of the atomic coordinates and lattice parameters of the *R*3*c* unit cell, and these were in turn refined (see Sec. A.1 in Ref. [33]). Because of the consideration of multiple cells to define the *A*-site disorder, we have the option of considering two separate lattice parameters for the bismuth-based bonds and sodium-based bonds. We can also consider separate atomic

TABLE I. Summary of different paths used in the refinement of room temperature EXAFS spectra of poled and unpoled NBT samples with the *R*3*c* structural model.

BiL_{III}-Edge		Ti K-Edge	
Path	Degeneracy	Path	Degeneracy
Bi-O1	3	Ti-O1	3
Bi-O2	3		
Bi-O3	3	Ti-O2	3
Bi-O4	3		
Bi-Ti1	1	Ti-Bi1	1
Bi-Ti2	3		
Bi-Ti3	3	Ti-Bi2	3
Bi-Ti4	1		
BiBi,BiNa	6	Ti-Bi3	3

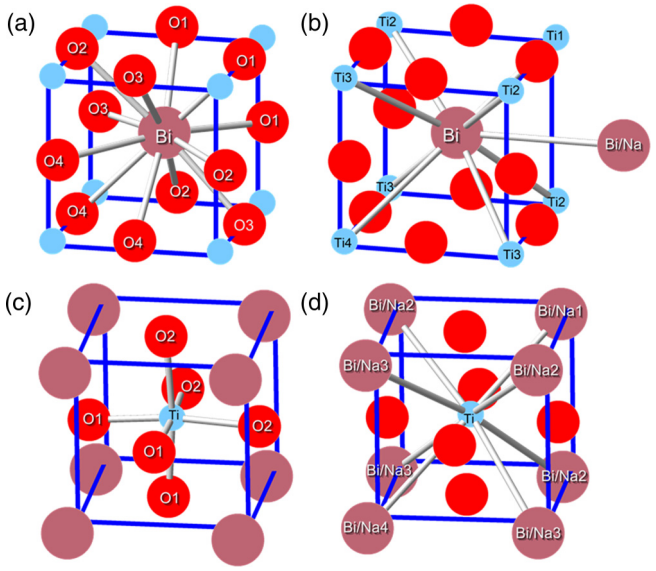

FIG. 3. A schematic of different paths used in the refinement of room temperature EXAFS spectra of NBT, with the *R*3*c* starting structural model. The pseudocubic cells are shown here for better visualization of (a) Bi-O bonds, (b) Bi-Ti, Bi-Bi and Bi-Na bonds, (c) Ti-O bonds, and (d) Ti-Bi and Ti-Na bonds.

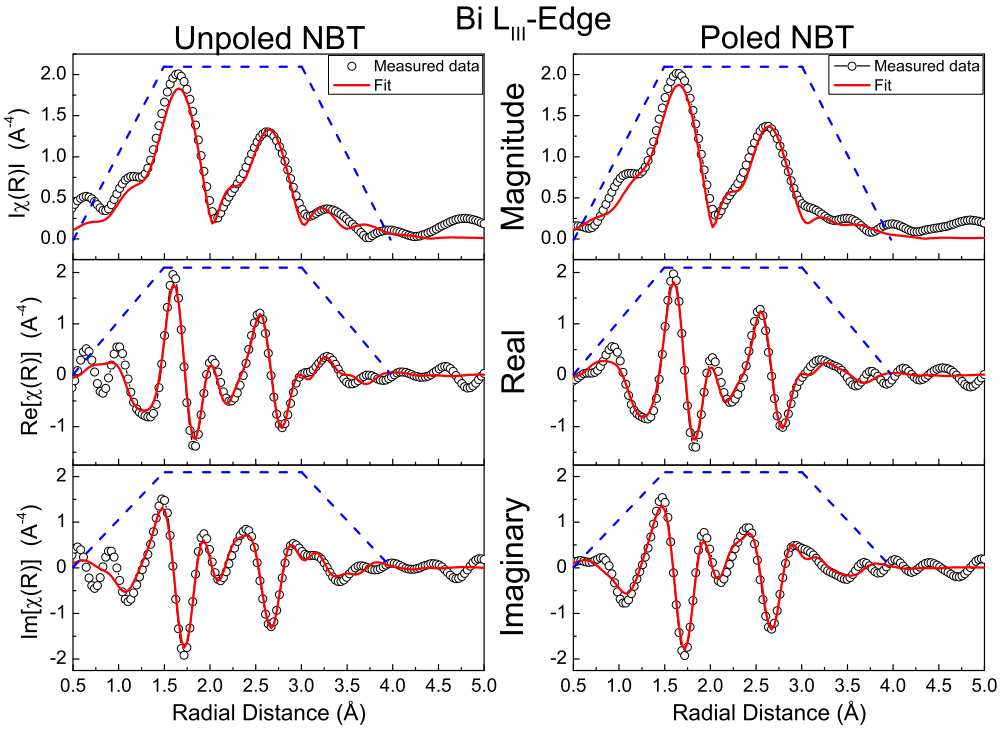

FIG. 4. Comparison of the room temperature Bi L_{III}-edge spectra of unpoled and poled NBT, fit with the $R3c$ model.

coordinates for the bismuth and sodium atoms. However, during the initial steps of the refinement, both the Bi cell and Na cell were forced to possess the same lattice parameters and coordinates. Only when the fit was improved close to that of the observed data were these allowed to be refined separately.

Figure 4 shows the best fit of the Bi L_{III}-edge EXAFS spectra with the $R3c$ model for both poled and unpoled samples. Both the samples show a reasonably good fit for the first two peaks. However, the subsequent broad peak around 3.5 Å is not well fit in both the poled and unpoled samples. Unfortunately, this is also the region where we see a significant difference in the poled and the unpoled samples. This region in the spectra accounts for the contribution by the Bi-Bi and Bi-Na bonds, and suggests that these bonds do not adhere to the rhombohedral distortion. It must also be noted that the spectra in this region could not be fit satisfactorily even if the symmetry constraints were relaxed, indicating there was a distribution of Bi-Bi and Bi-Na bond lengths. Hence, these bonds must be the root cause of the structural disorder in NBT, observed by other characterization techniques. The induced disorder seems like an intrinsic mechanism to accommodate the two different atoms in the A site. Also, the misfit observed even in the EXAFS spectra of the poled sample indicates that, at the cellular level, the Bi disorder is retained to some extent even after application of electric field. Figure 5 shows the fitting of the Ti K-edge EXAFS data with the $R3c$ model for the poled and unpoled samples. We can see that for both the samples, the fit is reasonably good for the considered range with the $R3c$ model, indicating that the Ti coordination favors a rhombohedral symmetry. Table II lists the results of the fitting and compares them for both the poled and the unpoled samples. Data from both the samples could be fit reasonably well with the $R3c$ model with R factors of 1.14% and 1.8% for the poled and unpoled samples, respectively. It can be seen from Table II that poling has noticeably altered the bond distances corresponding to the Bi coordination. On the other hand, there is no significant change corresponding to the distances associated with the Ti coordination, thereby confirming the observation in Sec. 3.1. The maximum change in the distances after poling is 0.01 Å in the Ti-O distance whereas one of the Bi-O distance decreased by 0.07 Å after poling. Even the rest of the bonds in the Ti coordination remain more or less unchanged after poling. Considering the fact that the data of the poled and the unpoled specimens were treated and analyzed in exactly the same fashion, and the error in the values of the bond distances are in the range of ±0.02 Å, any variation in distance greater than 0.02 in the Bi coordination can be treated to be outside of the error limit. Our result proves that the Ti-coordination environment is very rigid and is not affected by the application of electric field.

B. Temperature-dependent EXAFS on poled NBT

It has been observed from x-ray and neutron diffraction experiments that the structure of poled sample shows a sharp discontinuity at the depolarization temperature (T_d) of 200 °C [20]. At this temperature, the sample begins to deviate from the poled structural state and transforms to the unpoled state. This transition is also highlighted by appearance of long-range in-phase octahedral tilts in the system as well as a discontinuity in the evolution of the rhombohedral cell parameters [20]. We carried out temperature-dependent EXAFS measurements on the poled specimen to capture the signature of local structural rearrangement associated with the depolarization temperature,

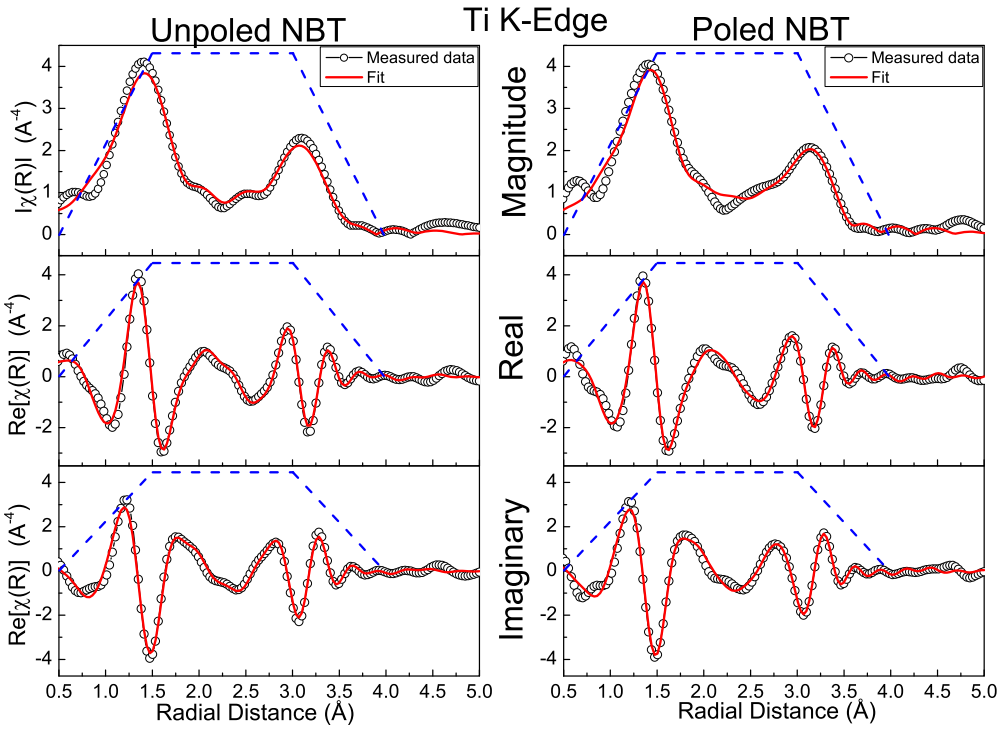

FIG. 5. Comparison of the room temperature Ti K-edge spectra of unpoled and poled NBT, fit with the $R3c$ model.

if any. EXAFS spectra for both Bi L_{III}-edge and Ti K-edge were collected at four different temperatures, namely, 150°, 250°, 300°, and 400 °C [Fig. 6]. Visual observation of Fig. 6 shows that with increasing temperature, the first peak in the Ti K-edge spectra (Ti-O bonds) shows only a slight decrease in intensity, as compared to the other peaks. The reason for this is likely that statistical disorder contributes largely to the decrease in the intensity of the other peaks, while this contribution is likely to be absent for the Ti-O bonds. It is known that while the structure below T_d is rhombohedral ($R3c$), the tetragonal phase emerges above T_d and manifests completely at 300 °C [20]. Hence, we tried to fit the spectra from all four temperatures by constraining them to both $R3c$ and $P4bm$ structural symmetry. The starting parameters of the $R3c$ structure was obtained from the results of the fitting of the room temperature EXAFS spectra of the poled NBT specimen, whereas that for $P4bm$ structure it was obtained from Rietveld analysis of neutron diffraction pattern of NBT at 400 °C [20]. We then sought to see how the two models would compare with each other, and if this could indicate the nature of the local structural symmetry at different temperatures. However, it was not possible to refine the EXAFS data constrained with the $P4bm$ model, and any attempt in doing so resulted in an unstable variation in the Bi-O and Ti-O bonds with unreasonable values. Even the

TABLE II. Comparison of the refinement result of room temperature EXAFS spectra of poled and unpoled NBT samples with the $R3c$ structural model.

		Poled NBT	Unpoled NBT
	Number of Independent points ($\mathbf{N_I}$)	26.2	26.2
	Number of Variables	18	18
	R-factor	1.14%	1.80%

Bi	Poled NBT (Å)	Unpoled NBT (Å)	Ti	Poled NBT (Å)	Unpoled NBT (Å)
Bi-O1	2.23	2.27	Ti-O1	1.91	1.91
Bi-O2	2.42	2.49	Ti-O2	2.07	2.08
Bi-O3	3.15	3.15	Ti-Bi1	3.06	3.04
Bi-O4	3.31	3.37	Ti-Bi2	3.26	3.26
Bi-Ti1	3.06	3.04	Ti-Bi3	3.44	3.52
Bi-Ti2	3.26	3.26	Ti-Na1	3.51	3.44
Bi-Ti3	3.44	3.52	Ti-Na2	3.40	3.40
Bi-Ti4	3.62	3.82	Ti-Na3	3.33	3.33
Bi-Bi1	3.86	3.91			
Bi-Na1	3.90	3.88			

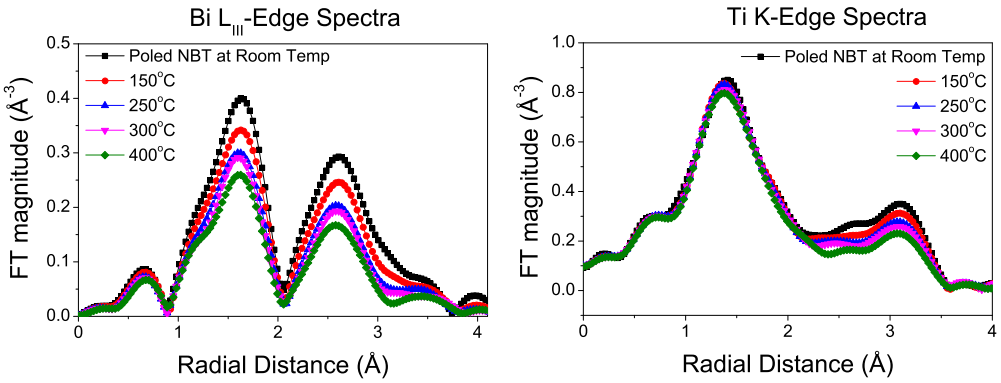

FIG. 6. High temperature evolution of the Bi L_{III}-edge and Ti K-edge EXAFS spectra of poled NBT.

refinement of the data with the $R3c$ model was not satisfactory. The reason for the inability to fit the spectra with either the $P4bm$ or $R3c$ structural model is attributed to the substantial increase in the positional disorder around and above the depolarization temperature. This disorder causes the deviation of the local structure from any particular symmetry, and hence constraining the fit to adhere to the $P4bm$ or $R3c$ symmetry was not a sensible choice.

We thus chose to approach the problem in a simpler way, i.e., by using the $P4bm$ structural model for obtaining only the initial theoretical EXAFS spectrum. The different paths were then allowed to be refined independently, without any symmetry constraints. The intensity of the peaks in an EXAFS spectrum can decrease either due to increasing disorder or decreasing coordination number. Here, the coordination number for each path, however, was fixed to that given by the $P4bm$ symmetry for all the spectra. Since it is known that the perovskite framework of the system is maintained at all the temperatures, it is reasonable to consider the decrease in the intensity of the peaks with temperature to be contributing solely from the statistical and thermal disorder. In comparison to the $R3c$ structure, the $P4bm$ starting model was more suited for this approach because of the lesser number of paths involved in the refinement. Also, for refinement with the $R3c$ starting model, a minimum of 31 variables was required, which is higher than the number of independent points (N_I) available here, which is equal to 26.26. In the case of the $P4bm$ model, only 25 variables are needed, thereby satisfying the Nyquist criteria. Though this approach cannot comment on the local symmetry of the system, one can still obtain valuable information on the evolution of different bond lengths as a function of temperature. Even in this case, a combined refinement of the Bi L_{III}-edge and Ti K-edge spectra were carried out so that the Bi-Ti path lengths could be kept common in the refinement. Table III gives the summary of different paths used for the refinement, and these paths can be visualized from Fig. 7.

All the patterns at different temperatures, including the room temperature patterns of poled and unpoled NBT were fit by this approach. A summary of the refinement results showing the evolution of the bond lengths, MSDs, and so on with temperature is given in the supplementary section [33]. We can notice two changes in the trend of the bond lengths; one between 150° and 250 °C and the other one between 300° and 400 °C, which are illustrated in Fig. 8 for selected bond lengths. In bulk structural characterization, we have a corresponding structural transition at both these temperatures. At 200 °C we have the depolarization taking place with introduction of local disorder in the octahedral tilts, whereas at 300 °C we have the structure transforming to a pure tetragonal $P4bm$ phase. These results clearly establish a correlation between the local structure and the bulk structural transition in NBT.

IV. DISCUSSION

The global structure of NBT is generally considered as rhombohedral ($R3c$), consisting of $a^-a^-a^-$ octahedral tilt and cations/anions displaced parallel to the polar [111] pseudocubic direction. This structure is compatible with the long-range ferroelectric state, as in rhomboehdral PZT and $BiFeO_3$. However, in contrast to a sharp dielectric anomaly expected for a ferroelectric-paraelectric transition, the temperature-dependent dielectric (ε'-T) measurements of NBT shows a weak hump at ~200 °C, and a diffuse anomaly at ~300 °C. While the anomaly at 300° C has generally been called as the Curie point, the polarization of NBT disappears above 200 °C. The considerable frequency dispersion of permittivity at 200 °C in the ε'-T plot of NBT led it to be characterized as a relaxor ferroelectric. However, unlike the canonical relaxor ferroelectric $Pb(Mg_{1/3}Nb_{2/3})O_3$, which exhibits a cubic-like

TABLE III. Summary of different paths used in the refinement of high temperature EXAFS spectra of poled NBT sample, with the $P4bm$ starting structural model.

BiL$_{III}$-Edge		Ti K-Edge	
Path	Degeneracy	Path	Degeneracy
BiO1	4	TiO1	1
BiO2	4	TiO2	4
BiO3	4	TiO3	1
BiTi1	4	TiBi1	4
BiTi2	4	TiBi2	4
BiBi1	4	TiTi1	6
BiBi2	2	TiNa1	4
BiNa1	4	TiNa2	4
BiNa2	2		

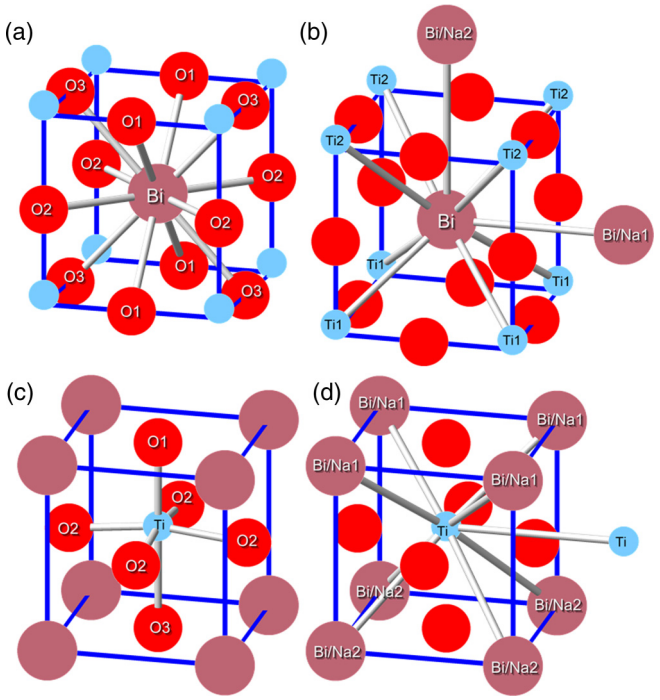

FIG. 7. A schematic of different paths used in the refinement of high temperature EXAFS spectra of poled NBT, with the $P4bm$ starting structural model. The pseudocubic cells are shown here for better visualization of (a) Bi-O bonds, (b) Bi-Ti, Bi-Bi and Bi-Na bonds, (c) Ti-O bonds, and (d) Ti-Bi and Ti-Na bonds.

global structure and slim ferroelectric hysteresis loop, the global structure of NBT has been known to be rhombohedrally distorted, and it shows a broad ferroelectric hysteresis loop, characteristic of a normal ferroelectric. The analysis of x-ray diffuse scattering experiment by Kreisel *et al.* [3] showed the presence of structural disorder and its relationship to the relaxor ferroelectricity in NBT. The authors proposed displacement of the A-site cations away from the polar [111] direction and towards ⟨100⟩, leading to a local monoclinic distortion. While electron diffraction patterns of NBT also show diffuse streaks, suggesting some kind of positional disorder [17,19], in addition, they also reported the occurrence of ½{ooe} superlattice spots, where o and e correspond to odd and even integers, respectively [16,18]. These superlattice spots are attributed to the presence of $a^0a^0c^+$ octahedral tilts, corresponding to the $P4bm$ structure, the coherence length of which is about ∼1–2 nm [19]. Levin and Reaney have postulated an assemblage of $a^0a^0c^+$ and $a^-a^-a^-$ tilts, giving an average tilt configuration $a^-a^-c^-$, which is consistent with the monoclinic (Cc) space group shown in some of the recent high-resolution diffraction studies [10,11]. The fact that poling field irreversibly suppresses the diffuse streaks as well as the ½{ooe} superlattice spots in electron diffraction patterns, and also suppresses the features in the XRD pattern corresponding to the Cc distortion, proved that the Cc-like global distortion is intimately related to the presence of structural entities with nanosized spatial coherence [20,27,28].

Since XRD study shows that the Cc distortion disappears completely after poling, and the structure appears as perfectly rhombohedral ($R3c$) [Fig. 9] [27,28], we would expect the

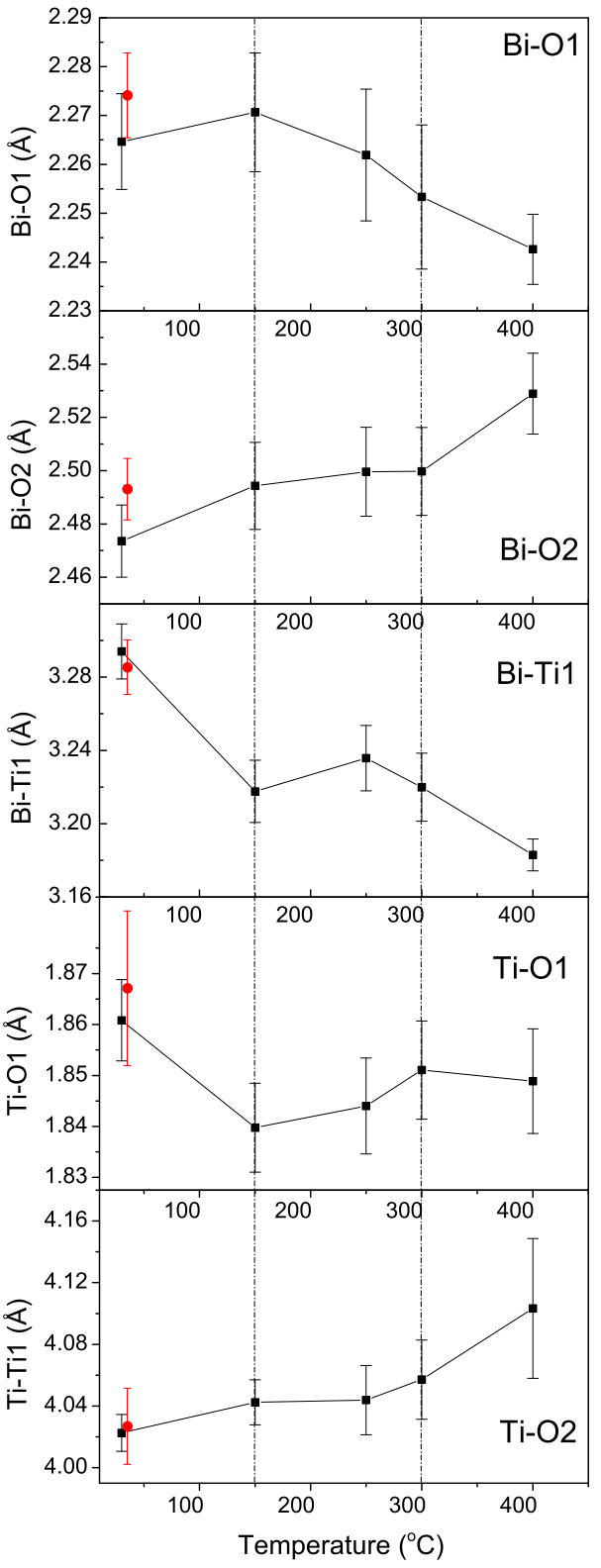

FIG. 8. Variation of selected bond lengths with temperature, as obtained by the refinement of EXAFS spectra. The additional red points in the figure correspond to the bond lengths of the annealed sample at room temperature.

Bi-O bond lengths of the poled sample to show identical values in both XRD and EXAFS analysis. Table IV displays the lattice-parameters and relevant bond lengths as obtained

TABLE IV. Rhombohedral ($R3c$) structural parameters obtained from Rietveld refinement of XRD data of poled NBT at room temperature, discussed in a previous paper [27].

Atom	x	y	z	$\mathbf{B}/\beta_{ij}(\text{Å}^2)$
Na/Bi	0	0	0.27933(2)	$\beta_{11} = 0.0268(5)$ $\beta_{33} = 0.0017(4)$ $\beta_{12} = 0.0134(2)$
Ti	0	0	0.01328(7)	1.06(5)
O	0.1223(7)	0.3416(7)	0.08330*	0.71(9)

a = 5.47801(5) Å; **c** = 13.5559(1) Å

$\boldsymbol{R_p} = 2.60$; $\boldsymbol{R_{wp}} = 3.84$; $\boldsymbol{\chi^2} = 3.60$;

*O(z) fixed to deal with floating origin.

	Bi	Poled NBT (Å)	Ti	Poled NBT (Å)
Bond Lengths	Bi-O1	2.432(4)	Ti-O1	1.897(4)
	Bi-O2	2.505(4)		
	Bi-O3	3.031(4)		
	Bi-O4	3.124(4)		
	Bi-Ti1	3.172(7)		
	Bi-Ti2	3.292(2)	Ti-O2	2.041(4)
	Bi-Ti3	3.437(3)		
	Bi-Ti4	3.606(7)		
	Bi-Bi1	3.887(3)		
	Bi-Na1	3.887(3)		

by Rietveld analysis of poled NBT sample (shown in Fig. 9). A comparison of Tables II and IV clearly shows that the shortest Bi-O bond length of 2.2 Å predicted by EXAFS is still not obtained by the Rietveld analysis of XRD of poled sample. This anomaly leads to the conclusion that even though poling forces the A-site cations to align in the pseudocubic [111] direction, the Bi atoms are still underbonded, and hence they try to achieve a lower bond length of 2.2 Å wherever possible. In addition, this anomaly was found to persist even at higher temperatures. The shortest bond-length determined from x-ray diffraction of the pattern at 400 °C was again greater by ∼0.4 Å, than that predicted by the EXAFS spectra at the same temperature.

A further comparison of Tables II and IV shows that that most of the other bond lengths predicted by EXAFS match reasonably well with that predicted by XRD. Since the Ti-O bonds are unaffected by the poling field (Table II), the oxygen octahedra surrounding the Ti atom can be considered to be rigid. In this scenario, a local octahedron would respond by tilting to minimize the overall stress field induced due to local A-site positional disorder. It seems plausible from these results that the fundamental factor responsible for the appearance of in-phase tilted octahedra with nanoscale spatial coherence is A-site cation displacements away from the polar [111] direction. The electric field brings about positional order on the A site by aligning them along the polar direction of the $R3c$ phase; an inference which is also supported by the x-ray total scattering studies by Usher *et a.l* [21]. The fact that this alignment is retained even after removal of the poling field suggests that the system prefers the long-range positional order, and that some kind of kinetic factor prevents the realization of this long-range order initially. The positional disorder in the unpoled specimen can be attributed to the combined effect of quenched chemical disorder and differing bonding characteristics of Bi and Na with oxygen. These randomly quenched Na and Bi atoms are expected to induce strain on a local scale, irrespective of the average structure of NBT on the global scale. When this strain increases due to additional chemical disorder, as in the case of Ba-substituted NBT compositions, the system adopts a long period modulation [34,35]. It may also be noted that the appearance of superlattice peaks characteristic of the in-phase octahedral tilt has been reported even in the globally cubic high temperature phase [20,36], indicating the intrinsic nature of the system to tend towards tilt disorder. The departure from the cubic phase at high temperature was also observed by Shuvaeva *et al.* in their Ti K-edge XANES data, which showed no significant reduction in the Ti off-center displacement up to temperatures as high as 600° C [4].

A visual examination of Fig. 6 shows that, while the peaks in Bi L_{III}-edge spectra show considerable decrease in intensity

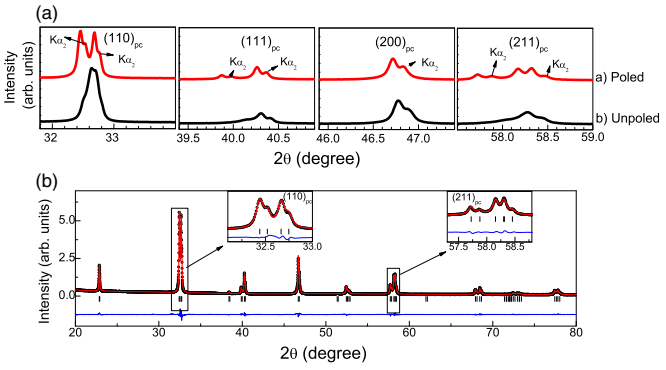

FIG. 9. (a) Comparison of room temperature XRD patterns of unpoled and poled NBT sample. (b) Rietveld refinement of the XRD pattern of poled NBT sample with $R3c$ space group model.

with increasing temperature, there is only a slight decrease in the first peak of the Ti K-edge spectra, which corresponds to the signal from the Ti-O bonds. In any real system, the mean square displacement term has contribution from both static disorder caused by the distribution in the bond lengths, and dynamic disorder caused by thermal vibrations of absorbing and scattering atoms. The observation in Fig. 6 suggests that the Ti-O octahedra remains rigid even at higher temperatures, and the slight decrease in the Ti-O peak is only due to the thermal vibrations. In contrast, the considerably greater decrease in the Bi-O peak intensity in Bi L_{III}-edge spectra indicates that there is continuous rearrangement of the Bi-atoms with temperature, thereby contributing to the static disorder. The σ^2 obtained from the fitting of the EXAFS spectra shows an increase from 0.0048 to 0.0064 for the Ti-O1 shell, and from 0.0077 to 0.0141 for the Bi-O shell when heated from room temperature to 400° C (see supplementary information) [33], indicating a major contribution of statistical disorder in the Bi-O shell. It is thus clear that electric field and temperature mainly affect the displacement of Bi atoms, and tilting of the rigid Ti-O octahedra seems to accommodate the strain caused by this displacement. Since the local in-phase tilt is structurally incompatible with the $R3c$ ferroelectric distortion, they act as a kinetic barrier and hinder the development of a long-range polar order. The strong coupling of the electric field with polarization helps in overcoming the incompatible local structural distortions, and displaces the atoms along directions which are compatible with the long-range ferroelectric order. Because the intrinsic tendency for positional disorder is always present in the system, the field-induced positional order is lost again at the depolarization temperature, as is evident from the discontinuous change in the Bi-O bond length across the depolarization temperature [Fig. 8]. The local polarization may, however, still persist up to the Curie point which is $\sim$300 °C.

V. CONCLUSION

In this paper, we carried out a detailed local structure analysis of poled and unpoled $Na_{1/2}Bi_{1/2}TiO_3$ using Bi L_{III}-edge and Ti K-edge EXAFS. This study revealed that poling field affects the bond distances corresponding to the Bi coordination and not the Ti coordination. In view of our results, we argue that the monoclinic-like global distortion reported in NBT is primarily due to the positional disorder of the A-site cations. The occurrence of local in-phase octahedral tilt, often reported in the transmission electron microscopy (TEM) studies, seems to be associated with the minimization of the local strain field, induced by the A-site positional disorder. We also show a distinct change in the bond length corresponding to the Bi coordination as the poled specimen is heated through the depolarization temperature, further verifying that the positional disorder of the A-site cations is the fundamental factor for bringing about structural complexity and relaxor ferroelectric behavior in unpoled NBT.

ACKNOWLEDGMENTS

R.R. acknowledges Science and Engineering Board (SERB) of the Department of Science and Technology, Government of India for financial assistance (SERB/F/5046/2013-14). The authors from India thank ICTP, Trieste, Italy for the travel support for carrying out the experiments at ELETTRA.

[1] G. A. Smolenskii, V. A. Isupov, A. I. Agranovskaya, and N. N. Krainik, Sov. Phys. Solid State **2**, 2651 (1961).
[2] G. O. Jones and P. A. Thomas, Acta Crystallogr. B **58**, 168 (2002).
[3] J. Kreisel, P. Bouvier, B. Dkhil, P. A. Thomas, A. M. Glazer, T. R. Welberry, B. Chaabane, and M. Mezouar, Phys. Rev. B **68**, 014113 (2003).
[4] V. A. Shuvaeva, D. Zekria, A. M. Glazer, Q. Jiang, S. M. Weber, P. Bhattacharya, and P. A. Thomas, Phys. Rev. B **71**, 174114 (2005).
[5] A. M. Balagurov, E. Y. Koroleva, A. A. Naberezhnov, V. P. Sakhnenko, B. N. Savenko, N. V. Ter-Oganessian, and S. B. Vakhrushev, Phase Trans. **79**, 163 (2006).
[6] D. S. Keeble, E. R. Barney, D. A. Keen, M. G. Tucker, J. Kreisel, and P. A. Thomas, Adv. Funct. Mater. **23**, 185 (2013).
[7] E. Aksel, J. S. Forrester, J. C. Nino, K. Page, D. P. Shoemaker, and J. L. Jones, Phys. Rev. B **87**, 104113 (2013).
[8] P. A. Thomas, S. Trujillo, M. Boudard, S. Gorfman, and J. Kreisel, Solid State Sci. **12**, 311 (2010).
[9] G. O. Jones, J. Kreisel, and P. A. Thomas, Powder Diffr. **17**, 301 (2002).
[10] E. Aksel, J. S. Forrester, J. L. Jones, P. A. Thomas, K. Page, and M. R. Suchomel, Appl. Phys. Lett. **98**, 152901 (2011).
[11] S. Gorfman and P. A. Thomas, J. Appl. Crystallogr. **43**, 1409 (2010).
[12] S. Gorfman, A. M. Glazer, Y. Noguchi, M. Miyayama, H. Luo, and P. A. Thomas, J. Appl. Crystallogr. **45**, 444 (2012).
[13] W. Ge, C. P. Devreugd, D. Phelan, Q. Zhang, M. Ahart, J. Li, H. Luo, L. A. Boatner, D. Viehland, and P. M. Gehring, Phys. Rev. B **88**, 174115 (2013).
[14] A. M. Glazer, Acta Crystallogr. B **28**, 3384 (1972).
[15] A. M. Glazer, Acta Crystallogr. Sect. A **31**, 756 (1975).
[16] V. Dorcet, G. Trolliard, and P. Boullay, Chem. Mater. **20**, 5061 (2008).
[17] V. Dorcet and G. Trolliard, Acta Mater. **56**, 1753 (2008).
[18] V. Dorcet, G. Trolliard, and P. Boullay, J. Magn. Magn. Mater. **321**, 1758 (2009).
[19] I. Levin and I. M. Reaney, Adv. Funct. Mater. **22**, 3445 (2012).
[20] B. N. Rao, R. Datta, S. S. Chandrashekaran, D. K. Mishra, V. Sathe, A. Senyshyn, and R. Ranjan, Phys. Rev. B **88**, 224103 (2013).
[21] T.-M. Usher, I. Levin, J. E. Daniels, and J. L. Jones, Sci. Rep. **5**, 14678 (2015).
[22] B. Ravel and M. Newville, J. Synchrotron Radiat. **12**, 537 (2005).

[23] M. Newville, P. Līviņš, Y. Yacoby, J. J. Rehr, and E. A. Stern, Phys. Rev. B **47**, 14126 (1993).
[24] B. Ravel, J. Synchrotron Radiat. **8**, 314 (2001).
[25] J. J. Rehr and R. C. Albers, Rev. Mod. Phys. **72**, 621 (2000).
[26] J. J. Rehr, J. J. Kas, M. P. Prange, A. P. Sorini, Y. Takimoto, and F. Vila, C. R. Phys. **10**, 548 (2009).
[27] B. N. Rao and R. Ranjan, Phys. Rev. B **86**, 134103 (2012).
[28] B. N. Rao, A. N. Fitch, and R. Ranjan, Phys. Rev. B **87**, 060102 (2013).
[29] *X-Ray Absorption: Principles, Applications, Techniques of EXAFS, SEXAFS, and XANES,* edited by D. C. Koningsberger and R. Prins (Wiley, London, 1988).
[30] S. L. Lin, E. A. Stern, A. J. Kalb, and Y. Zhang, Biochemistry (Mosc.) **30**, 2323 (1991).
[31] J. J. Rehr, J. Mustre de Leon, S. I. Zabinsky, and R. C. Albers, J. Am. Chem. Soc. **113**, 5135 (1991).
[32] S. Calvin, *XAFS for Everyone* (Taylor & Francis, New York, 2013).
[33] See Supplemental Material at http://link.aps.org/supplemental/10.1103/PhysRevB.93.024106 for information on (i) fitting of room temperature EXAFS spectra with $R3c$ and $P4bm$ space group constraints, and (ii) the fitting results of the high temperature EXAFS spectra.
[34] R. Garg, B. N. Rao, A. Senyshyn, and R. Ranjan, J. Appl. Phys. **114**, 234102 (2013).
[35] B. N. Rao, D. K. Khatua, R. Garg, A. Senyshyn, and R. Ranjan, Phys. Rev. B **91**, 214116 (2015).
[36] G. Trolliard and V. Dorcet, Chem. Mater. **20**, 5074 (2008).